

## TOWARDS PROCESSING OF MULTILAYERED METALLIC MATERIALS – CONSTRAINED COMPRESSION TESTING

SZYMON BAJDA\*, MICHAŁ KRZYŻANOWSKI, MARCIN KWIECIEŃ, JANUSZ MAJTA,  
ŁUKASZ LISIECKI, JAKUB SROKA

*AGH University of Science and Technology, Faculty of Metals Engineering and  
Industrial Computer Science, Mickiewicza 30, 30-059 Krakow, Poland*

*\*Corresponding author: sbajda@agh.edu.pl*

### Abstract

The complex analysis of the interface behaviour has been performed during constrained compression testing of 316L steel plates as a way towards processing of the multilayered nanostructured metallic materials. The approach is based on a combination of experiments under appropriate operating conditions and computer modelling based on finite element (FE) methodology for interpretation of the test results. Multilayered metallic structure was successfully obtained using the constrained compression testing technique. The specially designed die and compression specimens allowed for joining of the steel plates together even at room temperatures. The performed numerical analysis using the ABAQUS/Standard FE software revealed the strain and stress localisation areas within the multilayered structure among other features that are described in the paper. The results are in agreement with experimental observations.

**Key words:** multilayered metallic materials, constrained compression test, numerical modelling, 316L stainless steel, stress and strain distribution

### 1. INTRODUCTION

Individual metallic components can be joined together to form a new single element with different mechanical properties. Such multilayered materials have increasing number of applications. They can be used, for instance, as evaporator plates for heat exchangers used in refrigerators and solar heat panels, as materials for cookware, for vehicle bumpers, for architectural purposes, for coins, for button cell batteries, for automotive slide bearings, for chemical and nuclear industries, for fuel cell electrodes and for other applications (Bay et al., 1985; Li et al., 2008). The most common processes used to manufacture these materials are the following: fusion welding, mechanical fastening and adhesive bonding. The welding process allows for achievement of higher bond strength comparing with other mentioned processes (Mori et al., 2013). In fusion weld-

ing the external heat source is utilized in order to melt the material near the interface. The quality and reliability of such obtained joint may be decreased by influence of high temperatures. There is a need for developing a new, lower cost and greater productivity bonding methods allowing for obtaining durable joining between two materials, which are usually different materials.

Alternatively to fusion welding, plastic deformation can be used for joining components without an external heat application. The group of processes allowing joining by plastic deformation includes cold welding by rolling, extrusion, forging, etc. Cold welding is a solid-state bonding process using pressure to tie metals together. Fundamentals of this process are described elsewhere (Milner & Rowe, 1962; Mori et al., 2013).

In cold welding, the bond can be established when two clean surfaces come into direct contact with themselves. The noticeable differences in weldability of numerous materials result from presence of contaminated films on the surface of these materials (Conrad & Rice, 1970; Sherwood & Milner, 1969). The surface preparation is required in order to remove the contaminations and obtain successful bonding. The most commonly used method is degreasing followed by scratch-brushing, which plays an additional and important role along with the cleaning function, namely, it creates a work hardened, brittle covering layer on the material surface (Bay, 1983). This layer arises directly on the surface of metal, so that the oxide scale cannot come into intimate contact with metal in these areas. During deformation the cover layer breaks and the pressure causes extrusion of the not oxidised metal through appearing cracks omitting the contaminant film (figure 1). This leads to direct contact between virgin metal surfaces resulting in bonding establishment (Bay, 1983).

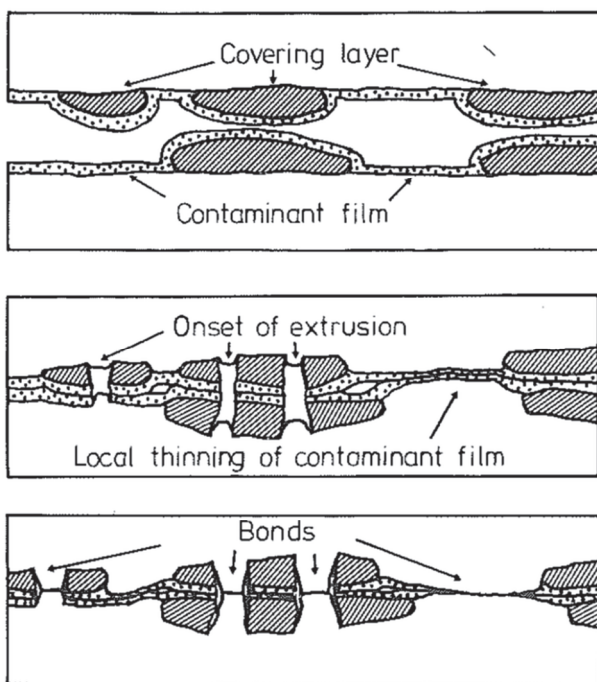


**Fig. 1.** Bonding mechanism during cold welding for scratch-brushed surfaces (Bay, 1986).

The quality of bonding can be evaluated visually by using optical and scanning electron microscopy (Ghafari-Gousheh et al., 2015) or mechanically, using peeling test (Manesh & Shahabi, 2009). Additionally, the peeling test allows for determination of bond strength.

Nowadays, manufacture of multilayered materials with refined grains is becoming more common.

In the last two decades, nanostructured materials attracted widespread interest due to their superior mechanical properties, such as high yield and ultimate strengths comparing to the analogous polycrystalline coarse-grained metals and alloys (Gleiter, 1989; Roland et al., 2007; Roland et al., 2009). However, their ductile properties are much lower, which is directly related to the volume fraction of the refined grains in these materials (Chen et al., 2005; Muszka et al., 2007). Ultrafine-grained structures can be obtained by using of various severe plastic deformation (SPD) processes, such as Accumulative Roll Bonding (ARB), Equal Channel Angular Extrusion (ECAE) or High Pressure Torsion (HPT). Moreover, it has been proved that recently developed Surface Mechanical Attrition Treatment (SMAT) is able to refine the grains in the surface layer to the nanometre scale (Lu & Lu, 1999; Roland et al., 2005; Roland et al., 2006). SMAT allows for obtaining bulk materials with limited depth of refined grains at the surface layer, which is not sufficient for enhancement of their mechanical properties and usually cause rapid saturation of the yield strength (Waltz et al., 2009b). Mechanical properties can be improved through increase of the volume fraction of the refined grains. Combining SMAT technique used for grain refining at the surface layer of the material with subsequent thermomechanical processing (TMP) allows for obtaining metallic materials with multilayered bulk structure and the increased volume fraction of the refined grains. TMP is used for joining of the nanostructured metallic platters together. Such duplex techniques can be used to produce materials for structural applications with enhanced yield and ultimate strength, while conserving an acceptable elongation to failure. However, bonding imperfections between platters can result in significant deterioration of mechanical properties of such multilayered materials. Among the reasons of weakening the interfaces are impurities deposited on the surface and interfacial oxidation that is more pronounced at elevated temperatures (Bajda et al., 2015; Waltz et al., 2009a).

The bonding strength depends on many various parameters, such as a material type, surface preparation, surface roughness, scratch-brushing parameters, delay time between surface preparation and bonding process itself (Jamaati & Toroghinejad, 2011; Pawlicki et al., 2015; Quadir et al., 2008; Yanagimoto et al., 2010). Nanostructures at the surface layer make the bonding even more complicated. This is due to the different properties of the refined



grain structures and altered interactions between them comparing with their coarse-grained counterparts. Additionally, interfacial oxidation occurs during TMP at high temperatures, which causes bonding imperfections and makes materials joining much more difficult. Moreover, the diffusion rate within the nanostructured surface layers is higher than for coarse-grained materials due to the increased grain boundary density (Ralston & Birbilis, 2010). This has a dual effect on corrosion behaviour that depends on the external environment. An improvement of the corrosion resistance of the nanostructured surface layers has been reported in passivating electrolytes, while a decrease has been shown in depassivating electrolytes (Gupta & Birbilis, 2015; Liu et al., 2010). Furthermore, SMAT introduces surface defects (e. g., cracks), which has deleterious effect on corrosion performance. However, low temperature annealing can be applied to such materials to remove the surface imperfections causing some improvement of oxidation resistance compared to coarse-grained materials (Wang & Li, 2002; Wang & Li, 2003).

metallic materials. In order to be able to compare behaviour of nanostructured material with coarse-grained one, the goal of this first step of the project is to obtain joint between coarse-grained metallic parts via the developed compression technique and to analyse material response during the processing. In order to avoid influence of high temperature oxidation on the interfaces, compression tests were performed at room temperature. A specially designed hollow die and rounded tools were used. Numerical simulation based on FE methodology was applied in order to examine the details of material behaviour. The Abaqus/Standard FE software was used for the calculations. Strain and stress localisations were identified and discussed in the work.

## 2. EXPERIMENTAL PROCEDURE – CONSTRAINED COMPRESSION TEST

The constrained compression test was carried out on hydraulic press of maximum capacity 5000 kN at room temperature and without lubrication. Eight cylindrically-shaped plates of 1 mm thickness and 10 mm diameter were cut by using

**Table 1.** Chemical composition of 316L stainless steel used in research.

Element	C	Si	Mn	P	S	Cr	Ni	Mo	N
Content, [%]	0.02	0.488	0.9	0.0315	0.0002	16.998	11.039	2.03	0.0287

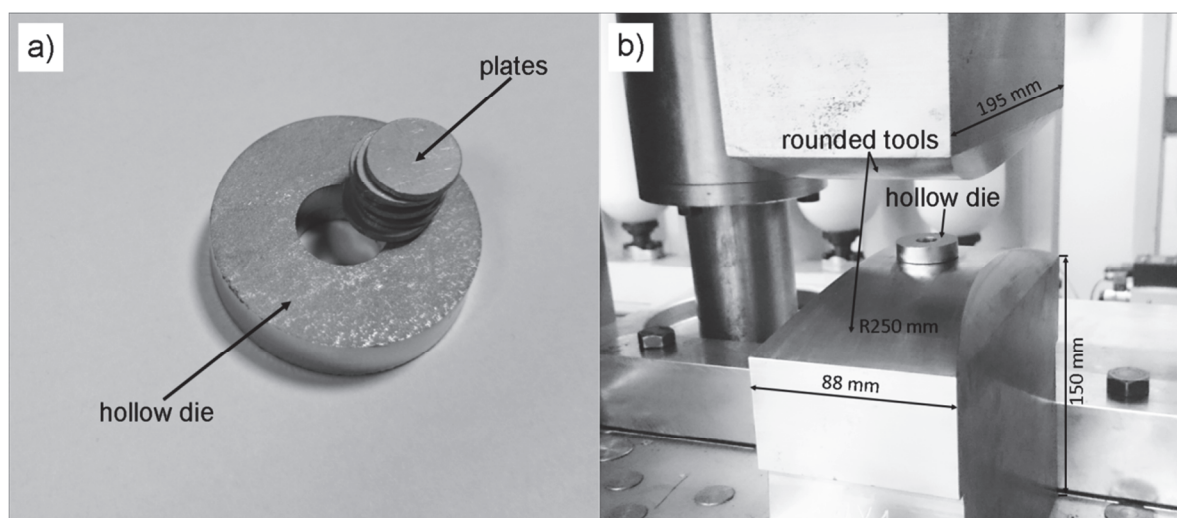


**Fig. 2.** a) Steel plates and hollow die before the compression; b) experimental set-up.

In the present study, the constrained compression testing technique was applied for bonding of 316L stainless steel platters together. The aim of the whole project, which is divided by consecutive stages, is better understanding of the highly reactive interfaces behaviour of nanostructured multilayered

waterjet cutting technique from 316L stainless steel cold rolled sheet with 20-50  $\mu\text{m}$  initial grain size and chemical composition presented in table 1.

The hollow die of 8 mm thickness, 30 mm outer diameter and 10 mm inner diameter was cut by laser also from 316L steel. After placing the plates into



the hollow die (figure 2a), the package was undergoing compression between the specially designed rounded tools with 45% and 55% reduction (figure 2b). The indicated values were obtained at the centre of such package, where reduction level is the highest.

The bottom tool was fixed during compression while the speed of the top tool was chosen to be 7.2 mm/s. The radius, height, width and length of the tools were the following: 250, 150, 88 and 195 mm respectively. The rounded tool shape changing the deformation conditions within the compressed package allowed for generation of the relevant shearing necessary for bonding at the interfaces (Quadir et al., 2008). The specifically designed tool shape also allowed for reduction of forces required for such compression, therefore higher reduction levels were achieved using the same testing rig comparing with conventional forging.

shown earlier that the bond strength decreases with increase of delay times between the surface preparation and the joining process (Jamaati & Toroghinejad, 2011).

The compression load was applied simultaneously on the plates and the hollow die in this technique. The external constraint has a noticeable impact on material flow (Eskandari et al., 2013). Thus, the designed hollow die confining the material flow during the compression significantly disturbed the local deformations around the interfaces.

### 3. NUMERICAL MODELLING

3D FE based model of the constrained compression test has been developed and applied for the analysis (figure 3).

Eight cylindrically-shaped steel plates were placed one over another (figure 3b). The thickness

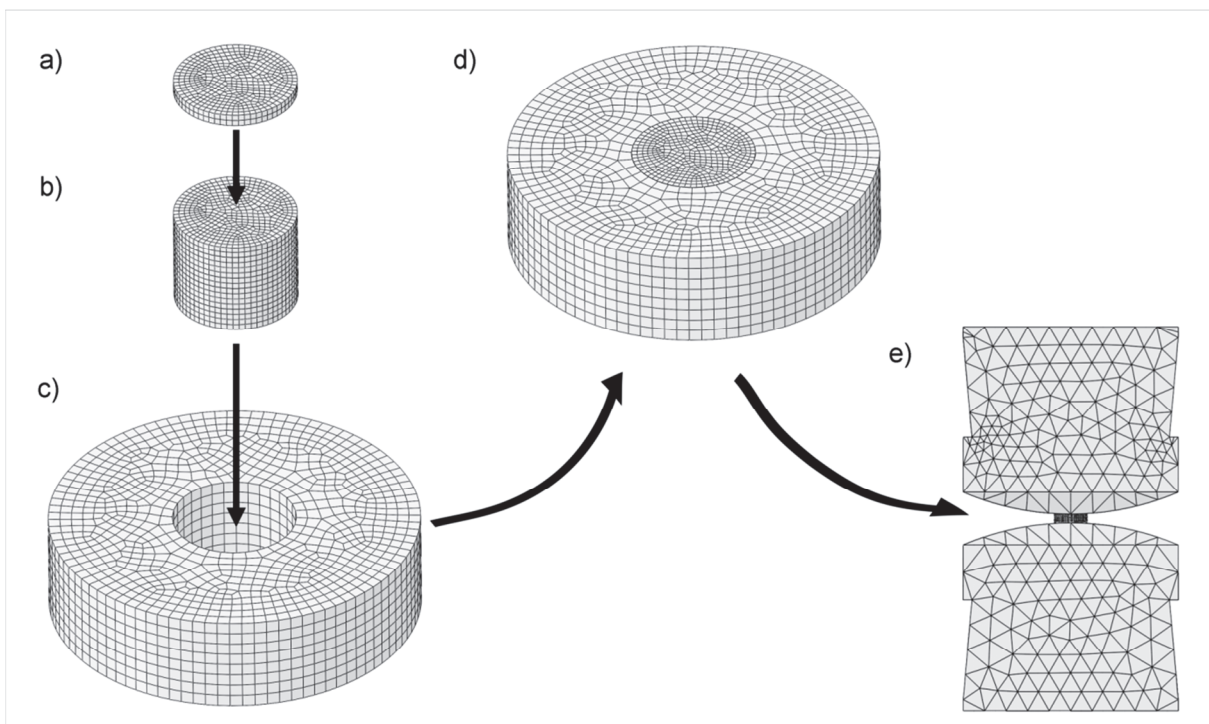


**Fig. 3.** Schematic representation of the FE model: a) single steel plate b) eight superposed plates c) hollow die d) plates inserted into the hollow die e) die with plates placed between rounded tools.

Before the specimens were subjected to the compression testing, all the plate surfaces were degreased with acetone and subjected to both sides scratch-brushing. Immediately after that, they were placed into the hollow die. Then, the package was undergoing compression without delay. The time interval between the scratch-brushing and the compression operation was less than a minute. The short time interval was necessary, because it has been

and diameter of each plate was 1 mm and 10 mm respectively, reflecting the actual sizes of the specimens. The hollow die thickness, the outer and inner diameter was 8 mm, 30 mm and 10 mm, respectively (figure 3c). The packed plates were inserted into the model of the die (figure 3d) and finally, the whole package was placed between the two rounded shape rigid tools, each of 250 mm radius, as it is shown in figure 3e.



The standard isotropic Coulomb friction model has been assumed in the numerical calculations. No relative motion between surfaces occurs if the equivalent frictional stress  $\tau_{eq}$  is less than the critical stress  $\tau_{cr}$ , which is proportional to the contact pressure, as it is shown in the following equations:

$$\tau_{eq} = \sqrt{\tau_1^2 + \tau_2^2} \quad (1)$$

$$\tau_{cr} = \mu p \quad (2)$$

where  $p$  is the contact pressure and  $\mu$  is the friction coefficient. The critical stress is defined as follows:

$$\tau_{cr} = \min(\mu p, \tau_{max}) \quad (3)$$

where  $\tau_{max}$  is an adjustable parameter. The slip occurs when the equivalent frictional stress reaches the critical stress value. The direction of the slip coincides with the frictional stress, which can be expressed by equation (4):

$$\frac{\tau_i}{\tau_{eq}} = \frac{\gamma_i}{\gamma_{eq}} \quad (4)$$

where  $\gamma_i$  is the slip rate in  $i$  direction and  $\gamma_{eq}$  is the equivalent slip velocity:

$$\gamma_{eq} = \sqrt{\gamma_1^2 + \gamma_2^2} \quad (5)$$

The condition of no relative motion between the surfaces that come into contact is approximated by stiff elastic behaviour. Therefore, the relative motion from the zero shear stress position is determined by a critical slip  $\gamma_{cr}$  value, which was set as 0.5% of the average length of all contact elements.

plates and the tools surfaces,  $\mu = 0.35$ , and between the die and the tool surfaces,  $\mu = 0.3$ .

The calculations were performed using the model consisting of 16342 elements including 5558 quadratic tetrahedral elements of type C3D10 representing the tool and 10784 linear hexahedral elements of type C3D8R representing the both plates and the die. The symmetric boundary conditions shown in figure 4 were applied for the modelling. The boundary conditions were the following:

- zero-X displacements for nodes lying on the YZ-plane ( $U_x = 0$ );
- zero-Y displacements for nodes lying on the XZ-plane ( $U_y = 0$ );
- zero-Z displacements for nodes lying on the XY-plane ( $U_z = 0$ ).

The same elastic-plastic material model with isotropic hardening has been chosen for both the plates and the hollow die. Its Young's modulus, Poisson's ratio and the yield stress were assumed as the following: 190 GPa, 0.3 and 290 MPa, respectively. The stress-strain relationship was introduced into the model as the following equation (Petit et al., 2012):

$$\sigma = 290 + 1255 \cdot \varepsilon^{0.733} \quad (6)$$

where  $\varepsilon$  is the effective plastic strain.

Various compression reductions from 18% to 55% have been applied during the numerical analysis.

The Newton-Raphson's method was chosen as a numerical technique for solving the nonlinear equilibrium equations primary due to better rate of convergence comparing to other methods.

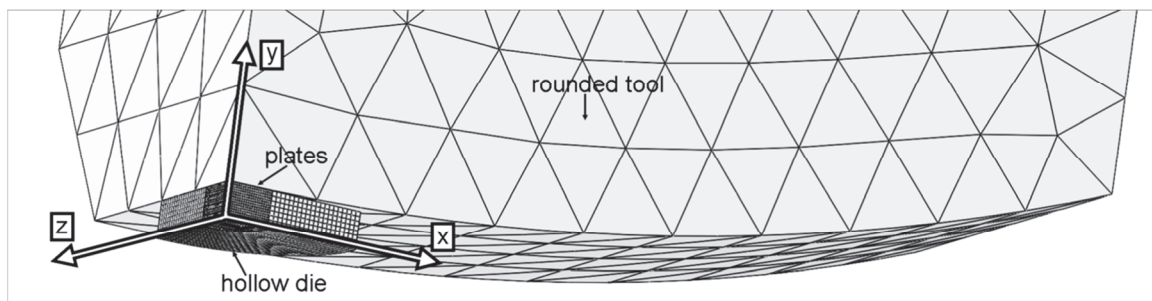


Fig. 4. 3D FE model set-up used for analysis.

The scratch-brushing operation changes the surface roughness, hence different friction coefficients have been assumed between the plate surfaces, such as  $\mu = 0.4$ , between the plate side surfaces and the hollow die inner surface,  $\mu = 0.3$ , between the outer

#### 4. RESULTS AND DISCUSSION

The cross-sections of the typical samples obtained after the constrained compression test along

with their model representation are presented in figure 5.

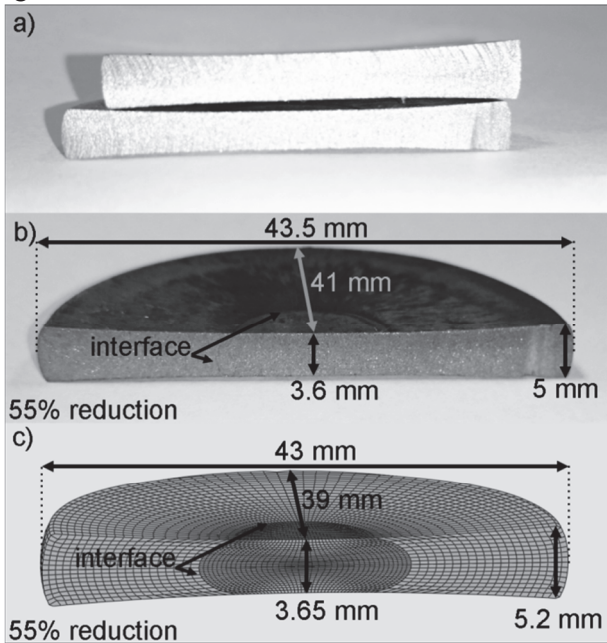


Fig. 5. Sample cross-sections after constrained compression test: a,b) experimental, c) FE model.

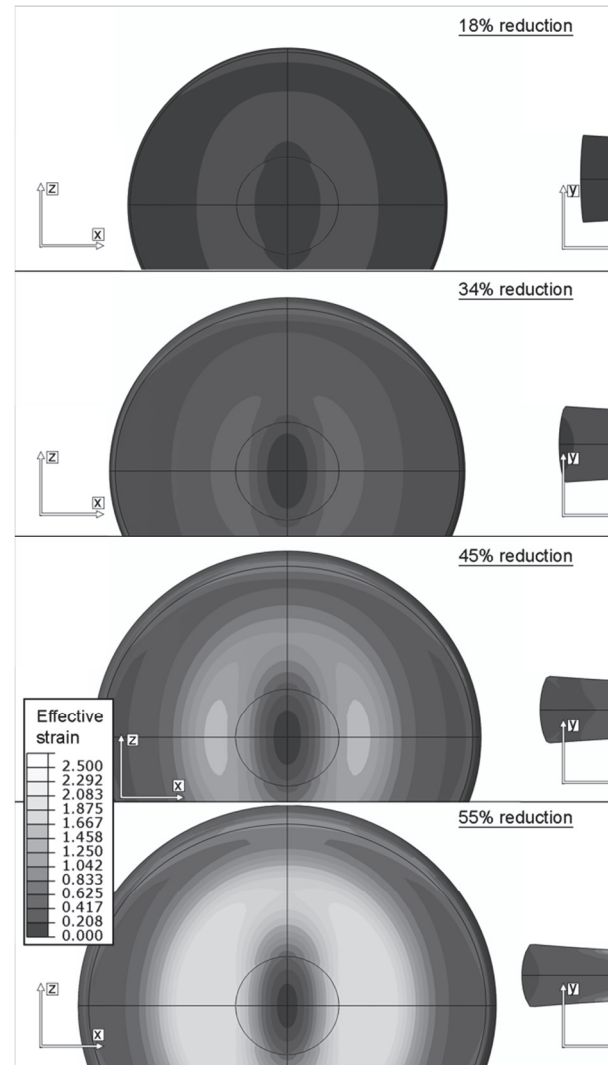


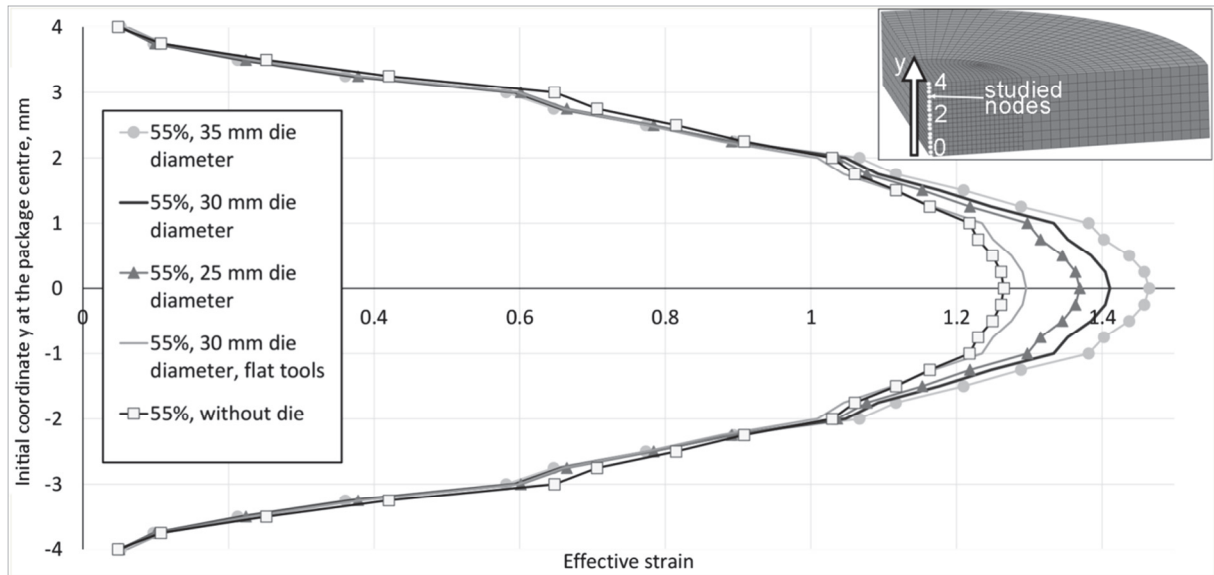
Fig. 6. The effective strain predicted at the package surface and the cross-section.

Figure 5a illustrates the compressed package using 45% (top) and 55% (bottom) reductions. The characteristic profile of the deformed package can be observed in the figure with lower thickness in the middle and the curved side surface due to barrelling. The similar shape and dimensions of the package were obtained during the numerical analysis (figure 5c). The experimentally obtained profile of the interface between the die and the plates also exhibits good agreement with the results of prediction (figure 5b and c) conforming to the conventional viewpoint that the material flows easier towards the sides at half height of the package thickness and its flow is more difficult near the top and bottom surfaces. This is due to the relatively high friction coefficient between the package and tool surfaces. The maximum pressing force achieved experimentally at 55% reduction was about 3500 kN, while the corresponding one obtained numerically was about 3300 kN.



No sliding between the plates was registered numerically when the hollow die was applied, while relative movement between the plates was noticeable during compression without the hollow die. This indicates that presence of the die improves the conditions required for obtaining successful bonding.

plate is placed within the package, the more pronounced is its reduction and, consequently, the larger is its diameter. This is due to the influence of the forces acting simultaneously from both top and bottom tools. The portion of the material at the top is pressed into the bottom one and vice versa. This



**Fig. 7.** The effective strain predicted at the nodes located across the thickness of the package on the symmetry axis for the different die diameters and tool shapes. One eighth of the model is shown at the upper right corner.

The effective strain predicted during the compression test for the consequent stages of 18%, 34%, 45% and 55% reduction is shown in figure 6. At the beginning of the process, the material is mostly deformed at the die surface, due to shear stresses resulted from the tool shape, and also in the middle of the package volume creating a characteristic cross-shaped pattern (figure 6a). In the following stage, as it is seen in figure 6b, the deformed earlier regions expand accumulating the strain. When compression reaches 45% reduction (figure 6c), the strain in the mentioned above surface areas exceeds the strain in the cross-section centre. When the reduction level reaches 55% (figure 6d), the effective strain increases significantly, especially in these top areas. It is due to higher shear stresses that are developed in the area during the whole process. The stresses are much higher than in the case of using flat tools (figure 8). The lowest deformation occurred directly in the middle of the surface at the place of the first contact with the tool. Even at such large reduction, the thickness of the outermost plates was similar to their initial thickness, in contrast to the thickness of the inner plates that were deformed significantly. It has to be mentioned that the closer to the middle the

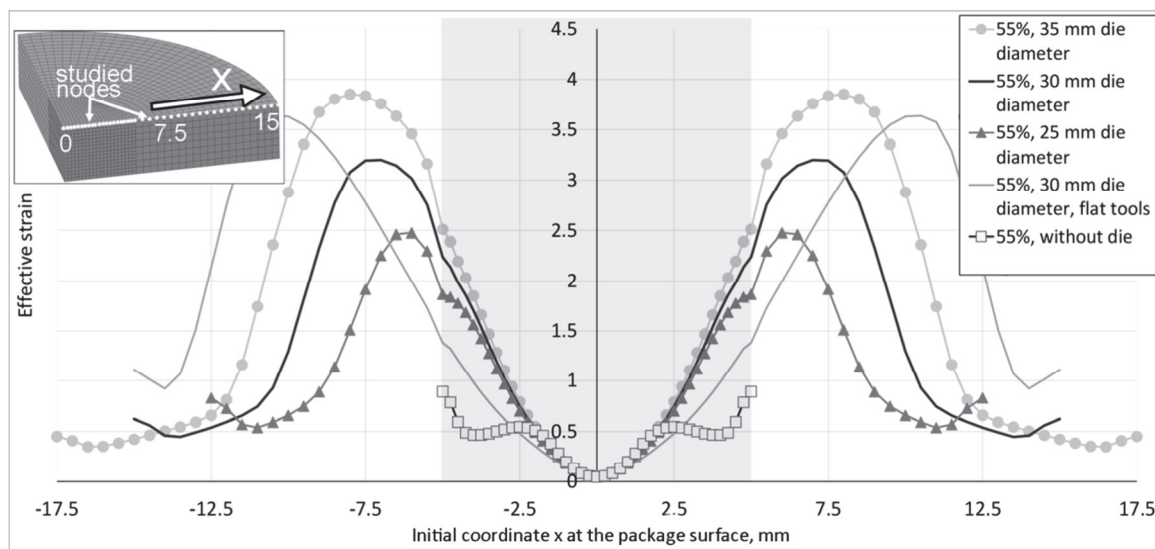
causes both high stresses at the interfaces in the middle of the package and large height reductions of the plates located in this region. The deformed material flows in X direction increasing the plates diameter. The phenomenon was also observed experimentally (figure 5b). The strain distribution observed within the plates favours the conclusion that the closer to the package centre the chances for successful bonding are higher. Furthermore, the grain size should be finer at these areas as well. The tools should also favour the grain refinement at lateral parts of the outer plates because of the direct contact between them and the plates under the deformation.

Figure 7 illustrates differences between the effective strain predicted at the nodes located at the sample centre for various geometry conditions of the sample and tools. Vertical axis corresponds to the initial Y coordinate of the nodes, while the effective strain is given for the nodes after deformation. Such way of presentation allows for placement of the results obtained for various conditions in the single graph. It can be seen that the closer to the sample centre, the higher effective strains are present. Generally, the highest values of the effective strain are obtained, if the following two conditions are satis-



fied: the contact surface of the tools is rounded and the hollow die is used for the constrained compression test. The specific tool shape favours generation of additional shear stresses, which contribute to the obtained effective strain values. A hollow die constrains the lateral expansion of the plates increasing in such way stresses within them that results in obtaining greater effective strains than for the case without the hollow die application. If the rounded tools are used without a hollow die, the corresponding effective strains become lower than in the case of using flat tools with the hollow die. Larger die outer diameters allow for achievement of larger deformations. Although, obtaining the same reductions requires higher pressures.

As can be seen in figure 8, the highest effective strains are achieved at the package surface when both 35 mm diameter die and the rounded tools are used. Smaller strains are obtained in the case of the flat tools. However, it has to be mentioned that in the second case, the large deformations occur not in the plate but in the die itself, at 8 mm distance from the plate centre. It results from the fact, that the flat tool surface acting uniformly on the whole package surface, while the stress influenced by application of the rounded tool surface is the highest at the centre and gradually decreases with the distance from the package centre. Thus, the pressure induced by the flat tool exceeds the one generated by the rounded tool at some distance from the centre causing the



**Fig. 8.** The effective strain predicted at the nodes located at the package surface along the symmetry axis for the different geometrical conditions. Grey colour area indicates coordinates of nodes representing plates.

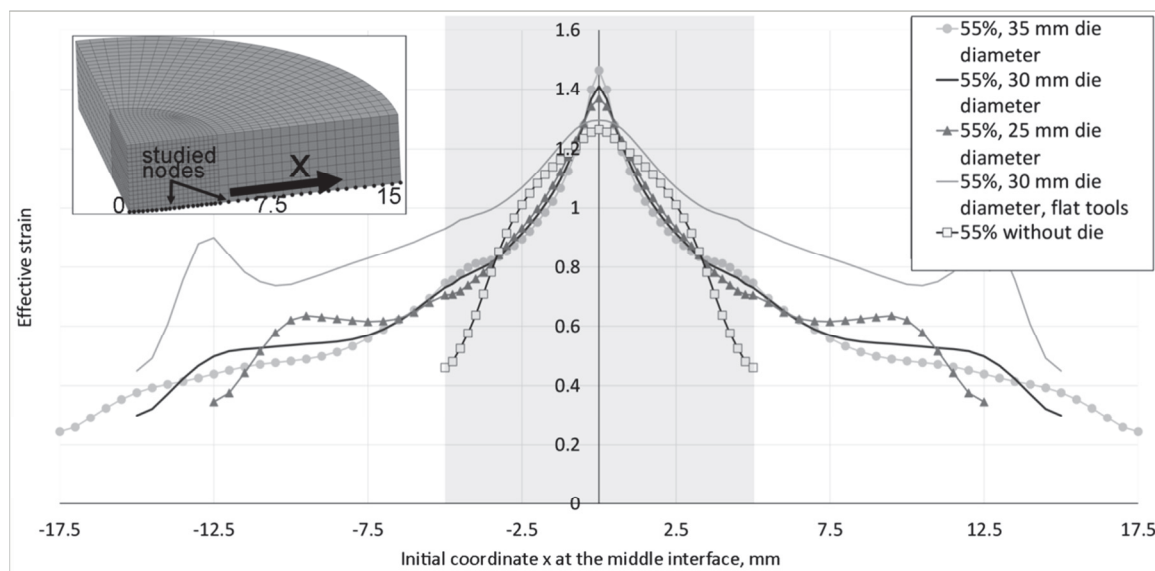


**Fig. 9.** The effective strain predicted at the nodes located on the symmetry axis at the interface situated at half-value thickness of the package.



observed high strains in the die. The deformations will have less noticeable effect on bonding between plates than in the cases when both the rounded tools and the hollow die are used simultaneously. When the hollow die is not used, the strain at the nodes doesn't grow as the distance from the centre increases above 2 mm. It favours the conclusion that the hollow die provides more beneficial conditions for obtaining reliable bonding between the platters in processing of multilayered metallic materials.

Figure 9 shows the effective strain predicted at the interface at half-value of the package thickness. It can be noticed that the largest deformations are achieved in the vicinity of the centre, namely, within 0.5 mm from the centre assuming both the hollow die and rounded tools are used. Similarly to the previous case, larger effective strains are observed when dies with larger outer diameters are used. The highest strains are achieved at distances longer than 0.5 mm from the centre in the case of using flat tools. At the same time, the lowest effective strains were predicted at the centre during compression without a die using rounded tools. They become higher at distances longer than 0.5 mm from the midpoint. However, the bonding was not obtained experimentally during compression without a die allowing for suggestion that obtaining high effective strains near the sample centre is the most significant for successful bonding.

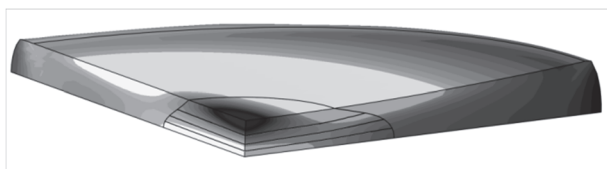


**Fig. 10.** Schematic representation of the effective stress localizations during constrained compression testing. (One-eighth of the package. Bright colour corresponds to higher stresses).

As it can be noticed from figure 10, the areas of the highest effective stresses are located mainly at the surface layer of the die and at the interface in the vicinity of the plate centre during the constrained compression test. It has to be mentioned, that the areas of the die surface layer, where the high stresses were observed, are vulnerable to cracking requiring reasonable accuracy during experimentation. Nevertheless, the described constrained testing procedure allows for detailed quantitative analysis of the micro events taking place at the interfaces during processing of multilayered metallic materials including evolution of the microstructure and events related to interface oxidation leading to better understanding

of mechanisms responsible for achievement of the desirable mechanical properties.

## 5. CONCLUSIONS

Development of the testing procedure leading to understanding of mechanisms responsible for processing of multilayered metallic materials is considered in this work paving the way towards processing of multilayered nanostructured metallic materials. The performed numerical analysis of strain and stress distributions within the package of eight cylindrically-shaped steel plates during constrained compression testing using the hollow die of different shapes supported by the relevant experimental results allowed for clarification of the specific role of the hollow die in terms of achievement a desirable stress (strain) state around the interfaces of the multilayered material. The numerical results are in good agreement with the available experimental evidence. Based on the observations and discussion above, the following conclusions can be drawn:

1. The hollow die significantly improved mechanical conditions at the interfaces allowing for obtaining successful bonding between steel platters during compression.
2. Achievement of the highest possible effective strains within the proximity to the centre of the package was critical for obtaining a successful bonding during the test.
3. The mentioned effective strains can be obtained using the hollow die and the rounded tools.
4. The larger the diameter of the hollow die, the larger effective strain at the sample centre can be achieved. Although, it would require higher pressures to achieve the same reduction.
5. The thickness of the outermost plates is reduced insignificantly in comparison with inner plates of the package during the test.

## ACKNOWLEDGEMENT

The support from the National Science Centre, Poland (grant no. DEC-2013/09/B/ST8/00141) is greatly appreciated.

## REFERENCES

- Bajda, S., Krzyzanowski, M., Muszka, K., Rainforth, W. M., 2015, Numerical analysis of highly reactive interfaces in processing of nanocrystallised multilayered metallic materials by using duplex technique, *Surf. Coatings Technol.*, 277, 170-180.



- Bay, N., 1983, Mechanisms Producing Metallic Bonds in Cold Welding, *Weld. Reseach Suppl.*, 62, 137-142.
- Bay, N., 1986, Cold welding: Part I Characteristics, bonding mechanisms, bond strength, *Met. Constr.*, 18(8,10), 369-372.
- Bay, N., Clemensen, C., Juelstorp, O., Wanheim, T., 1985, Bond Strength in Cold Roll Bonding, *CIRP Ann. - Manuf. Technol.*, 34(1), 221-224.
- Chen, X. H., Lu, J., Lu, L., Lu, K., 2005, Tensile properties of a nanocrystalline 316L austenitic stainless steel, *Scr. Mater.*, 52(10), 1039-1044.
- Conrad, H., Rice, L., 1970, The cohesion of previously fractured Fcc metals in ultrahigh vacuum, *Metall. Trans.*, 1(11), 3019-3029.
- Eskandari, M., Zarei-Hanzaki, A., Pilehva, F., Abedi, H. R., Fatemi-Varzaneh, S. M., Khalesian, A. R., 2013, Ductility improvement in AZ31 magnesium alloy using constrained compression testing technique, *Mater. Sci. Eng. A*, 576, 74-81.
- Ghafari-Gousheh, S., Hossein Nedjad, S., Khalil-Allafi, J., 2015, Tensile properties and interfacial bonding of multilayered, high-purity titanium strips fabricated by ARB process, *J. Mech. Behav. Biomed. Mater.*, 51, 147-153.
- Gleiter, H., 1989, Nanocrystalline materials, *Prog. Mater. Sci.*, 33(4), 223-315.
- Gupta, R. K., Birbilis, N., 2015, The influence of nanocrystalline structure and processing route on corrosion of stainless steel: A review, *Corros. Sci.*, 92, 1-15.
- Jamaati, R., Toroghinejad, M. R., 2011, The role of surface preparation parameters on cold roll bonding of aluminum strips, *J. Mater. Eng. Perform.*, 20(2), 191-197.
- Li, L., Nagai, K., Yin, F., 2008, Progress in cold roll bonding of metals, *Sci. Technol. Adv. Mater.*, 9(2), 1-11.
- Liu, L., Li, Y., Wang, F., 2010, Electrochemical Corrosion Behavior of Nanocrystalline Materials - a Review, *J. Mater. Sci. Technol.*, 26(1), 1-14.
- Lu, K., Lu, J., 1999, Surface nanocrystallization (SNC) of metallic materials-presentation of the concept behind a new approach, *J. Mater. Sci. Technol.*, 15(3), 193-197.
- Manesh, H. D., Shahabi, H. S., 2009, Effective parameters on bonding strength of roll bonded Al/St/Al multilayer strips, *J. Alloys Compd.*, 476(1-2), 292-299.
- Milner, D. R., Rowe, G. W., 1962, Fundamentals of Solid-Phase Welding, *Metall. Rev.*, 7(1), 433-480.
- Mori, K. I., Bay, N., Fratini, L., Micari, F., Tekkaya, A. E., 2013, Joining by plastic deformation, *CIRP Ann. - Manuf. Technol.*, 62(2), 673-694.
- Muszka, K., Majta, J., Hodgson, P. D., 2007, Study of the grain size effect on the deformation behavior of microalloyed steels, In *Proceedings of Materials Science And Technology*, Detroit MI: Association for Iron and Steel Industry 6, 493-504.
- Pawlicki, M., Drenger, T., Pieszak, M., Borowski, J., 2015, Cold upset forging joining of ultra-fine-grained aluminium and copper, *J. Mater. Process. Technol.*, 223, 193-202.
- Petit, J., Waltz, L., Montay, G., Reتراint, D., Roos, A., François, M., 2012, Multilayer modelling of stainless steel with a nanocrystallised superficial layer, *Mater. Sci. Eng. A*, 536, 124-128.
- Quadir, M. Z., Wolz, A., Hoffman, M., Ferry, M., 2008, Influence of processing parameters on the bond toughness of roll-bonded aluminium strip, *Scr. Mater.*, 58(11), 959-962.
- Ralston, K. D., Birbilis, N., 2010, Effect of grain size on corrosion, *Corrosion*, 66(7), 1-4.
- Roland, T., Reتراint, D., Lu, K., Lu, J., 2005, Generation of nanostructures on 316L stainless steel and its effect on mechanical behavior, *Mater. Sci. Forum*, 490-491, 625-630.
- Roland, T., Reتراint, D., Lu, K., Lu, J., 2006, Fatigue life improvement through surface nanostructuring of stainless steel by means of surface mechanical attrition treatment, *Scr. Mater.*, 54(11), 1949-1954.
- Roland, T., Reتراint, D., Lu, K., Lu, J., 2007, Enhanced mechanical behavior of a nanocrystallised stainless steel and its thermal stability, *Mater. Sci. Eng. A*, 445-446, 281-288.
- Roland, T., Ya, M., Reتراint, D., Lu, K., Lu, J., 2009, A New Multilayered Nanostructured Composite Material Produced by Assembling SMA-Treated Thin Plates, *J. Mater. Sci. Technol.*, 20(Supl.), 55-58.
- Sherwood, W. C., Milner, D. R., 1969, The Effect of Vacuum Machining on the Cold Welding of Some Metals, *J. Inst. Met.*, 97, 1-5.
- Waltz, L., Reتراint, D., Roos, A., Olier, P., 2009a, Combination of surface nanocrystallization and co-rolling: Creating multilayer nanocrystalline composites, *Scr. Mater.*, 60(1), 21-24.
- Waltz, L., Reتراint, D., Roos, A., Olier, P., Lu, J., 2009b, High Strength Nanocrystallized Multilayered Structure Obtained by SMAT and Co-Rolling, *Mater. Sci. Forum*, 614, 249-254.
- Wang, X. Y., Li, D. Y., 2002, Mechanical and electrochemical behavior of nanocrystalline surface of 304 stainless steel, *Electrochim. Acta*, 47(24), 3939-3947.
- Wang, X. Y., Li, D. Y., 2003, Mechanical, electrochemical and tribological properties of nano-crystalline surface of 304 stainless steel, *Wear*, 255(7-12), 836-845.
- Yanagimoto, J., Oya, T., Kawanishi, S., Tiesler, N., Koseki, T., 2010, Enhancement of bending formability of brittle sheet metal in multilayer metallic sheets, *CIRP Ann. - Manuf. Technol.*, 59(1), 287-290.

#### W KIERUNKU WYTWARZANIA WIELOWARSTWOWYCH MATERIAŁÓW METALICZNYCH – PRÓBA OGRANICZONEGO ŚCISKANIA

Streszczenie

Przeprowadzono kompleksową analizę ewolucji naprężeń i odkształceń w pobliżu granic rozdziału podczas ograniczonego ściskania płytek ze stali 316L w celu opracowania procesów wytwarzania wielowarstwowych materiałów metalicznych, w tym o budowie nanostrukturalnej. Przeprowadzone badania są oparte na połączeniu badań doświadczalnych w odpowiednich warunkach z modelowaniem komputerowym opartym o metodę elementów skończonych (MES) w celu interpretacji wykonywanych prób. Przeprowadzone badania pozwoliły na uzyskanie wielowarstwowej struktury metalicznej obserwowanej w przekroju poprzecznym próbek poddanych ograniczonemu ściskaniu. Specjalnie zaprojektowana matryca oraz próbki do ściskania pozwoliły na połączenie stalowych płytek nawet w temperaturze pokojowej. Przeprowadzona analiza numeryczna z wykorzystaniem oprogra-



mowania ABAQUS/Standard ujawniła obszary lokalizacji naprężeń i odkształceń wewnątrz wielowarstwowej struktury, a także inne elementy, które zostały opisane w pracy. Wyniki analizy numerycznej są zgodne z wynikami badań doświadczalnych.

---

*Received: February 4, 2016*

*Received in a revised form: March 31, 2016*

*Accepted: April 25, 2016*

